Superdeformed Λ hypernuclei from relativistic mean field models

Bing-Nan Lu,[1, 2] Emiko Hiyama,[3] Hiroyuki Sagawa,[3, 4] and Shan-Gui Zhou[1, 5]

[1]*State Key Laboratory of Theoretical Physics, Institute of Theoretical Physics,*
Chinese Academy of Sciences, Beijing 100190, China
[2]*Institut für Kernphysik, Institute for Advanced Simulation,*
and Jülich Center for Hadron Physics, Forschungszentrum Jülich, D-52425 Jülich, Germany
[3]*Nishina Center, RIKEN, Wako, Saitama, 351-0198, Japan*
[4]*Center for Mathematics and Physics, University of Aizu, Aizu-Wakamatsu, Fukushima 965-8580, Japan*
[5]*Center of Theoretical Nuclear Physics, National Laboratory of Heavy Ion Accelerator, Lanzhou 730000, China*
(Dated: July 30, 2017)

We study the superdeformed (SD) states and corresponding SD hypernuclei of Ar isotopes with the multidimensionally-constrained relativistic mean field (MDC-RMF) models which can accommodate various shape degree of freedom. We found that the density profiles of SD states in Ar isotopes show a strong localization with a ring structure near the surface, while the central part of the density is dilute showing a hole structure. This localization of SD density induces an appreciable deformation in the hyperon wave function and results in a large overlap between the core and the hyperon in the SD hypernuclei of Ar isotopes. Then the Λ separation energy of SD state becomes larger than that of normally deformed or spherical ground state. This feature is different from that found in other nuclei such as ^{32}S, ^{56}Ni, and ^{60}Zn in which the Λ separation energy of larger deformed state is smaller. In this context, the measurement of the Λ separation energy may provide an important information on the localization of the density profile of SD states.

I. INTRODUCTION

A Λ particle is free from the nucleon's Pauli exclusion principle in nuclei due to the strangeness degree of freedom. When a Λ particle is added to a nucleus, it lays deeply in the nucleus and many interesting phenomena were pointed out as the outcome. For instance, by an addition of a Λ particle into the p-shell nuclei which have an α clustering structure, there is a dynamical contraction of nuclear size and stabilization in the binding energy [1–4], which is called the glue like role of the Λ particle. However, the shrinkage effect is dependent on the states in the p-shell or sd-shell nuclei which have both α clustering states and shell-like compacting states. Namely, by the addition of a Λ particle, we have 20 % to 30 % nuclear shrinkage in the clustering states, while almost no shrinkage effect in shell-like states [5].

As an impurity in normal nuclei, it was pointed out that a hyperon also induces the change of the nuclear shape. The nuclear response to the addition of a Λ particle can be studied by examining the Λ separation energy (S_Λ). The dependence of S_Λ on the nuclear shape is an interesting topic. For example, it has been pointed out that the Λ separation energies in clustering states of some nuclei, e.g., $^{10}_\Lambda$Be, $^{13}_\Lambda$C, and $^{21}_\Lambda$Ne, are smaller by 1 to 3 MeV than those in shell-like compact states of corresponding hypernuclei from few-body models [6, 7] and antisymmetrized molecular dynamics (AMD) model [8].

Recently, the self-consistent mean field models, both Skyrme Hartree-Fock (SHF) and relativistic mean field (RMF) models, have been applied to study the deformation of p- and sd-shell Λ hypernuclei [9–13]. In most of the cases, the deformation of core nuclei and the corresponding hypernuclei are similar with the same sign. However, relativistic mean field models predict drastic changes of the deformation by the injection of a hyperon, e.g., in $^{13}_\Lambda$C and $^{29}_\Lambda$Si [10, 13]. Thus in general the polarization effect of hyperons is larger in RMF than Skyrme HF (SHF) models [11].

Beyond sd-shell nuclei, there are many interesting structure issues to study. One of them is that in some nuclei there exist superdeformed (SD) states which are characterized by the ratio 2:1 between the long and the short deformation axes in the coordinate space. In nuclei with $A \sim 40$, SD states have been observed experimentally [14–16] and the structure of these states has been extensively studied by mean field models [17–22].

A question related to the SD nuclei is, can the SD minima in normal nuclei persist after the injection of a hyperon? If the answer is yes, we have a further question, what happens about the nuclear responses in the normally deformed (ND) and SD states by the addition of a hyperon, say, a Λ? It is likely that the Λ separation energies in SD states are smaller than those in ND states because of smaller overlap between the Λ particle and SD core, as predicted for clustering states by the few-body or AMD models [6–8]. Especially, it has been pointed out that the Λ separation energies in SD states of Ca and Sc isotopes by the addition of a Λ particle are smaller than those of ND states by Isaka et al. [23]. However, it should be noticed that within the framework of mean field models, the wave functions of nuclear states might be localized [24, 25]. It would be interesting to investigate the energy gain by the addition of a Λ particle to such localized states by using mean field models.

Among many mean field models, in this work we

adopt the multidimensionally-constrained relativistic mean field (MDC-RMF) models which can accommodate various shape degrees of freedom [26] and have been used to study the shape of light hypernuclei [13] and the structure of heavy nuclei [27–29]. This paper is organized as follows. In Sec. II, we describe briefly the MDC-RMF model and the properties of the Λ-N interaction employed here. In Sec. III, the results and discussions are presented. A summary is given in Sec. IV.

II. THEORETICAL FRAMEWORK

Recently multidimensionally-constrained relativistic mean field (MDC-RMF) models were developed in order to treat the various shape degrees of freedom in atomic nuclei. In the MDC-RMF models, the RMF equations are solved in an axially deformed harmonic oscillator (ADHO) basis [30]. The MDC-RMF models have been extended to including the hyperons [13], where the Dirac equations for the nucleons and hyperons and the Klein-Gordon equations for mesons are solved in the ADHO representation, while the Coulomb field is solved by the Green's function method. Next we mention briefly the formalism of the MDC-RMF models, mostly those related to the Λ hyperon; the readers are referred to Ref. [26] for more details.

In the MDC-RMF models, the RMF functional can be one of the following four forms: the meson exchange or point-coupling nucleon interactions combined with the nonlinear or density-dependent couplings. The deformations $\beta_{\lambda\mu}$ with even μ can be considered simultaneously. In the present work we use the meson-exchange type interactions and only consider the axial and reflection symmetric shapes. Thus the projection of the total angular momentum on the symmetric z-axis, Ω, and the parity π are both conserved.

The starting point of the meson-exchange RMF models for hypernuclei is the covariant Lagrangian density

$$\mathcal{L} = \mathcal{L}_0 + \mathcal{L}_\Lambda, \qquad (1)$$

where $\mathcal{L}_0$ is the standard RMF Lagrangian density for the nucleons and mesons [31–37] and $\mathcal{L}_\Lambda$ is that for the hyperon,

$$\begin{aligned}
\mathcal{L}_\Lambda &= \bar{\psi}_\Lambda \left(i\gamma^\mu \partial_\mu - m_\Lambda - g_{\sigma\Lambda}\sigma - g_{\omega\Lambda}\gamma^\mu\omega_\mu \right) \psi_\Lambda \\
&\quad + \frac{f_{\omega\Lambda\Lambda}}{4m_\Lambda} \bar{\psi}_\Lambda \sigma^{\mu\nu} \Omega_{\mu\nu} \psi_\Lambda,
\end{aligned} \qquad (2)$$

where m_Λ is the mass of the Λ hyperon, $g_{\sigma\Lambda}$ and $g_{\omega\Lambda}$ are the coupling constants of the Λ hyperon with the scalar and vector meson fields, respectively. The last term represents the tensor coupling between the Λ hyperon and the ω field [38]. $\Omega_{\mu\nu}$ is the field tensor of the ω field defined as $\Omega_{\mu\nu} = \partial_\mu\omega_\nu - \partial_\nu\omega_\mu$. Couplings to the ρ meson and the photon vanishes for Λ hyperons which are neutral and isoscalar. In the RMF model, the $\Lambda - \Sigma^0$

mixing, which was important in reproducing simultaneously the binding energies of the s-shell hypernuclei (see, e.g., Refs. [39, 40]), is not included explicitly.

Under the mean field approximation, the single particle Dirac equation for Λ hyperons reads,

$$[\boldsymbol{\alpha} \cdot \boldsymbol{p} + \beta\left(m_\Lambda + S_\Lambda\right) + V_\Lambda + T_\Lambda]\psi_{\Lambda i} = \epsilon_i\psi_{\Lambda i}, \qquad (3)$$

with the scalar potential $S_\Lambda = g_{\sigma\Lambda}\sigma$, the vector potential $V_\Lambda = g_{\omega\Lambda}\omega$, and the tensor potential,

$$T_\Lambda = -\frac{f_{\omega\Lambda\Lambda}}{2m_\Lambda}\beta\left(\boldsymbol{\alpha} \cdot \boldsymbol{p}\right)\omega. \qquad (4)$$

The mesons fields σ, ω, and ρ are obtained by solving the Klein-Gordon equations with source terms. For example, the equation for the ω meson reads,

$$\left(-\nabla^2 + m_\omega^2\right)\omega = \left(g_\omega\rho_B^V + g_{\omega\Lambda}\rho_\Lambda^V\right) - \frac{f_{\omega\Lambda\Lambda}}{2m_\Lambda}\rho_\Lambda^j, \qquad (5)$$

where ρ_B^V and ρ_Λ^V are the isoscalar-vector densities for nucleons and hyperons and

$$\rho^j = i\boldsymbol{\partial} \cdot \left(\sum_i v_i\psi_i^\dagger\boldsymbol{\gamma}\psi_i\right), \qquad (6)$$

is the divergence of the current.

In this work we use the parameter set PK1 [41] for the N-N interaction. The Λ-N effective interaction is set to be PK1-Y1 which was adjusted to reproduce the observed binding energies and spin-orbit splittings of the Λ hyper nuclei [42, 43]. In PK1-Y1 the coupling constants for the Λ-N interaction are determined by the relations $g_{\sigma\Lambda} = 0.580\,g_\sigma$, $g_{\omega\Lambda} = 0.620\,g_\omega$, and $f_{\omega\Lambda\Lambda} = -g_{\omega\Lambda}$. The spurious motion due to the breaking of the translational invariance is treated by including the microscopic center of mass correction $E_{\text{c.m.}} = -\langle P^2\rangle/(2MA)$ in the total binding energy [41, 44, 45].

The pairing effects are included by the BCS approximation with a finite-range separable pairing interaction [46–48],

$$V(\boldsymbol{r}_1 - \boldsymbol{r}_2) = -G\delta(\tilde{\boldsymbol{R}} - \tilde{\boldsymbol{R}}')P(\tilde{\boldsymbol{r}})P(\tilde{\boldsymbol{r}}')\frac{1 - \hat{P}_\sigma}{2}, \qquad (7)$$

where G is the pairing strength, $\tilde{\boldsymbol{R}}$ and $\tilde{\boldsymbol{r}}$ are the center of mass and relative coordinate between the paired particles, respectively. $P(\tilde{\boldsymbol{r}})$ is a Gaussian shaped function,

$$P(\tilde{\boldsymbol{r}}) = \frac{1}{(4\pi a^2)^{3/2}}e^{-\tilde{r}^2/a^2}, \qquad (8)$$

where a is the effective range of the pairing force. In Ref. [46] the strength and range of the separable force are adjusted to reproduce the momentum dependency of the pairing gap in the nuclear matter calculated from the Gogny forces. In this work we adopt the parameter set that mimics the Gogny force D1S:

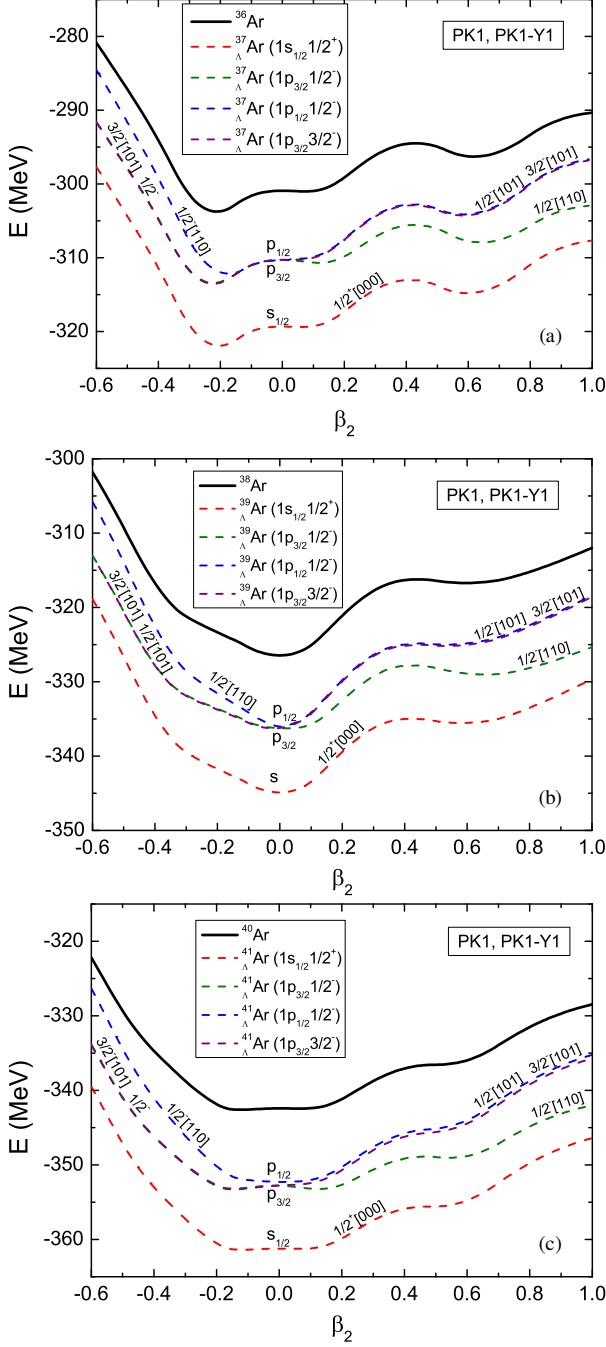$$G = 728.0 \text{ MeV} \cdot \text{fm}^3, \qquad a = 0.644 \text{ fm}. \qquad (9)$$

FIG. 1: The energy of (a) ^{36}Ar and $^{37}_{\Lambda}$Ar, (b) ^{38}Ar and $^{39}_{\Lambda}$Ar, and (c) ^{40}Ar and $^{41}_{\Lambda}$Ar as a function of the deformation parameter β_2, respectively. The Λ hyperon is injected into the lowest s orbit and three p orbits, respectively. The Nilsson quantum numbers $\Omega^{\pi}[Nn_3m_l]$ of the corresponding Λ orbits are marked.

III. RESULTS AND DISCUSSIONS

The calculated energy surfaces of several Ar isotopes (^{36}Ar, ^{38}Ar, and ^{40}Ar) and the corresponding Λ hypernuclei are shown in Fig. 1. The Λ hyperon is injected into

the lowest s orbit and three p orbits, respectively. The energy minimum of ^{36}Ar is found at the oblate side with $\beta_2 \sim -0.2$. The SD minimum is also found at $\beta_2 \sim 0.6$. The ground state of ^{38}Ar is spherical as seen in Fig. 1, while the SD state locates at deformation $\beta_2 \sim 0.6$ which is similar to that of ^{36}Ar. The energy surface of ^{40}Ar is rather flat around $\beta_2 \sim 0$ and the ground state is slightly oblate (see Table I). Around $\beta_2 \sim 0.5$, there is a shallow minimum.

The energy surfaces of hypernuclei $^{A+1}_{\Lambda}$Ar (a hyperon is put in the $1s_{1/2}$ or $\Omega^{\pi}[Nn_3m_l] = 1/2^+[000]$ states) with $A = 36$, 38, and 40 essentially follow those of the core nuclei ^{A}Ar. For instance, there are two minima for $^{37}_{\Lambda}$Ar, one at the oblate region and the other at the SD region. The SD minima become rather shallow in the cases $^{39}_{\Lambda}$Ar and $^{41}_{\Lambda}$Ar. Because of the small spin-orbit splitting of hyperon-nucleon interaction, the $1p_{1/2}$ and $1p_{3/2}$ states are almost degenerate in the limit of $\beta_2 = 0.0$. The $1/2^-[110]$ and $3/2^-[101]$ states are splitted in energy by the β_2 deformation in the similar way to the nuclear Nilsson levels while the $1/2^-[101]$ state is almost degenerate with $3/2^-[101]$ state because of the very small spin-orbit splitting in the Λ potential. Around $\beta_2 \sim 0.15$, there is a shoulder in the energy surface of ^{36}Ar. With one Λ added, this shoulder persists; when the Λ occupies the $1/2^-[110]$ state, a very shallow minimum even develops around $\beta_2 \sim 0.15$. In the following discussions, we will focus on the results in which the Λ hyperon occupies the $1/2^+[000]$ state.

The calculated deformations of ground states and SD states of several Ar isotopes are listed in Table I together with the root mean square (r.m.s.) radii, the binding energies, and the Λ separation energy defined by

$$S_{\Lambda} = E(^{A+1}_{\Lambda}\text{Ar}) - E(^{A}\text{Ar}). \qquad (10)$$

From Table I one finds some familiar features concerning the impurity effects of the Λ hyperon. First, the shrinkage effect appears in all these nuclei studied here as seen from the values of the r.m.s. radii. This effect is quite small for the ground states: The radius of a hypernucleus is smaller by less than 0.02 fm than that of the core nucleus. Even for the SD states, the change of the radius does not exceed 1%. Second, with A increasing, the radius of Λ hypernuclei increases, so does the r.m.s radius of the Λ distribution. Third, the shape of a Λ hypernucleus always follows its core nucleus and the addition of Λ does not change the sign of β_2. Finally, once the core is deformed, the density distribution of Λ is also distorted and the deformation parameter β_2 of a hypernucleus is always smaller than that of the corresponding core nucleus.

In Table I, we find that the Λ separation energies of Ar isotopes at the ground states have smaller values compared with those of the SD states, which is opposite to the case of lighter Λ hypernuclei such as $^{10}_{\Lambda}$Be [6, 7]. The $1/2^+_1$ state in ^{9}Be is much more deformed than the ground state $3/2^-_1$. When a Λ particle is added to these states, the Λ separation energy in ^{9}Be($1/2^+_1$) + Λ state is smaller than

TABLE I: The quadrupole deformation parameters, root mean square (r.m.s.) radii, binding energies, and Λ separation energies for the ground states and SD states (labelled with asterisks) in several Ar isotopes and the corresponding Λ hypernuclei. The experimental values of binding energies are taken from Ref. [49–51].

Nucleus	Quadrupole deformation parameters				R.m.s. radii (fm)		Energies (MeV)		
	β_2	β_n	β_p	β_Λ	r_m	r_Λ	E	E_{exp}	S_Λ
^{36}Ar	-0.212	-0.208	-0.215		3.238		-303.802	-306.716	
$^{37}_{\Lambda}$Ar	-0.204	-0.205	-0.211	-0.057	3.220	2.644	-321.979		18.177
^{38}Ar	0.000	0.000	0.000		3.281		-326.455	-327.343	
$^{39}_{\Lambda}$Ar	0.000	0.000	0.000	0.000	3.265	2.672	-344.896		18.441
^{40}Ar	-0.123	-0.112	-0.137		3.338		-342.613	-343.810	
$^{41}_{\Lambda}$Ar	-0.117	-0.109	-0.132	-0.037	3.321	2.698	-361.398		18.785
^{36}Ar*	0.620	0.610	0.630		3.346		-296.670		
$^{37}_{\Lambda}$Ar*	0.597	0.599	0.619	0.172	3.319	2.626	-315.194		18.524
^{38}Ar*	0.602	0.597	0.609		3.403		-317.448		
$^{39}_{\Lambda}$Ar*	0.589	0.596	0.603	0.187	3.378	2.659	-336.306		18.858
^{40}Ar*	0.499	0.472	0.533		3.430		-336.852		
$^{41}_{\Lambda}$Ar*	0.491	0.474	0.530	0.161	3.409	2.685	-355.922		19.070

TABLE II: Calculated deformation parameter β_2, the overlap $I_{overlap}$ defined in Eq. (11), the binding energy E, and Λ separation energy S_Λ of some Λ hypernuclei. For comparison, the binding energy of the core nucleus E_{core} is also given. The energies are in MeV.

Nucleus	β_2	$I_{overlap}$	E_{tot}	E_{core}	S_Λ
$^{37}_{\Lambda}$Ar	-0.204	0.1352	-321.979	-303.802	18.177
$^{37}_{\Lambda}$Ar*	0.597	0.1370	-315.194	-296.670	18.524
$^{39}_{\Lambda}$Ar	0.000	0.1360	-344.896	-326.455	18.441
$^{39}_{\Lambda}$Ar*	0.589	0.1378	-336.306	-317.448	18.858
$^{41}_{\Lambda}$Ar	-0.117	0.1357	-361.398	-342.613	18.785
$^{41}_{\Lambda}$Ar*	0.491	0.1378	-355.922	-336.852	19.070
$^{41}_{\Lambda}$Ca	0.00	0.1361	-361.422	-342.869	18.553
$^{41}_{\Lambda}$Ca*	0.70	0.1393	-350.559	-331.317	19.242
$^{33}_{\Lambda}$S	0.26	0.1376	-285.095	-267.002	18.093
$^{33}_{\Lambda}$S*	0.97	0.1243	-274.315	-257.951	16.364
$^{57}_{\Lambda}$Ni	0.00	0.1461	-506.665	-484.759	21.906
$^{57}_{\Lambda}$Ni*	0.40	0.1415	-498.610	-477.892	20.718
$^{61}_{\Lambda}$Zn	0.22	0.1438	-534.565	-512.924	21.641
$^{61}_{\Lambda}$Zn*	0.62	0.1415	-527.168	-506.238	20.930

that in ^{9}Be$(3/2_1^-) + \Lambda$ state. This has been explained as that the overlap between nucleons and the Λ hyperon in the $1/2_1^+$ state is smaller than that in the ground state. Next we will show that in Ar isotopes, however, the overlap between the nucleons and the Λ hyperon in the SD state is larger than that in the ground state, which results in a larger Λ separation energy in the SD state.

To clarify the physical mechanism of the larger Λ separation energy in the SD state, we calculate the overlap $I_{overlap}$ of the core and the hyperon,

$$I_{overlap} = \int \rho_{core}(r,z)\rho_\Lambda(r,z)rdrdz, \quad r = \sqrt{x^2+y^2}.$$
(11)

where the core and the hyperon densities are denoted by $\rho_{core}(r,z)$ and $\rho_\Lambda(r,z)$, respectively.

In Table II, the overlaps $I_{overlap}$ are listed together the

deformation parameter β_2, the binding energy E, and Λ separation energy S_Λ of some Λ hypernuclei. For $^{A+1}_{\Lambda}$Ar, one finds that the overlap $I_{overlap}$ in the SD state is always larger than that in the ground state. This explains well that the Λ separation energy in the SD state is larger than that of the ground state. In the following we will examine the density distributions of the core nucleus and the Λ hyperon and show that this new feature actually stems from a localized density of nucleons in the core nucleus and a stretched density of the Λ hyperon in the SD state.

We illustrate the calculated two-dimensional density distributions in the r-z plane (note that the z-axis is the symmetric one) for the ground and SD states in ^{36,38,40}Ar and $^{37,39,41}_{\Lambda}$Ar in Fig. 2. The ground states of ^{36}Ar and its hyper-counterpart $^{37}_{\Lambda}$Ar are clearly oblate. On the other hand, it is remarkable that the SD density distribution shows a clear localization feature with a ring shape near the surface and a hole structure with lower density at the center. Note that similar localization feature has been found and studied in details for the ground state of ^{20}Ne [24]. Furthermore, we see that as increasing number of neutrons, this localization with a ring shape of density profile becomes less pronounced as shown in Fig. 2. This behavior can also be deduced in β_2 values in Table I where one finds that, as the number of neutrons increases, the deformation β_2 becomes smaller. When a Λ particle is added to ^{36,38,40}Ar, the density profiles are almost similar with those of corresponding normal nuclei and the localization effect is still there. And also, as increasing the number of neutrons, the weakness of localization with a ring shape of density profile in hypernuclei is similar with those of the corresponding normal nuclei.

In Fig. 3 we show the two-dimensional density distributions in the r-z plane for the Λ hyperon in the ground and SD states of $^{37}_{\Lambda}$Ar. It is seen that in the ground of $^{37}_{\Lambda}$Ar, the Λ hyperon distributes almost isotropically; this is consistent with the small β_Λ value given in Table I.
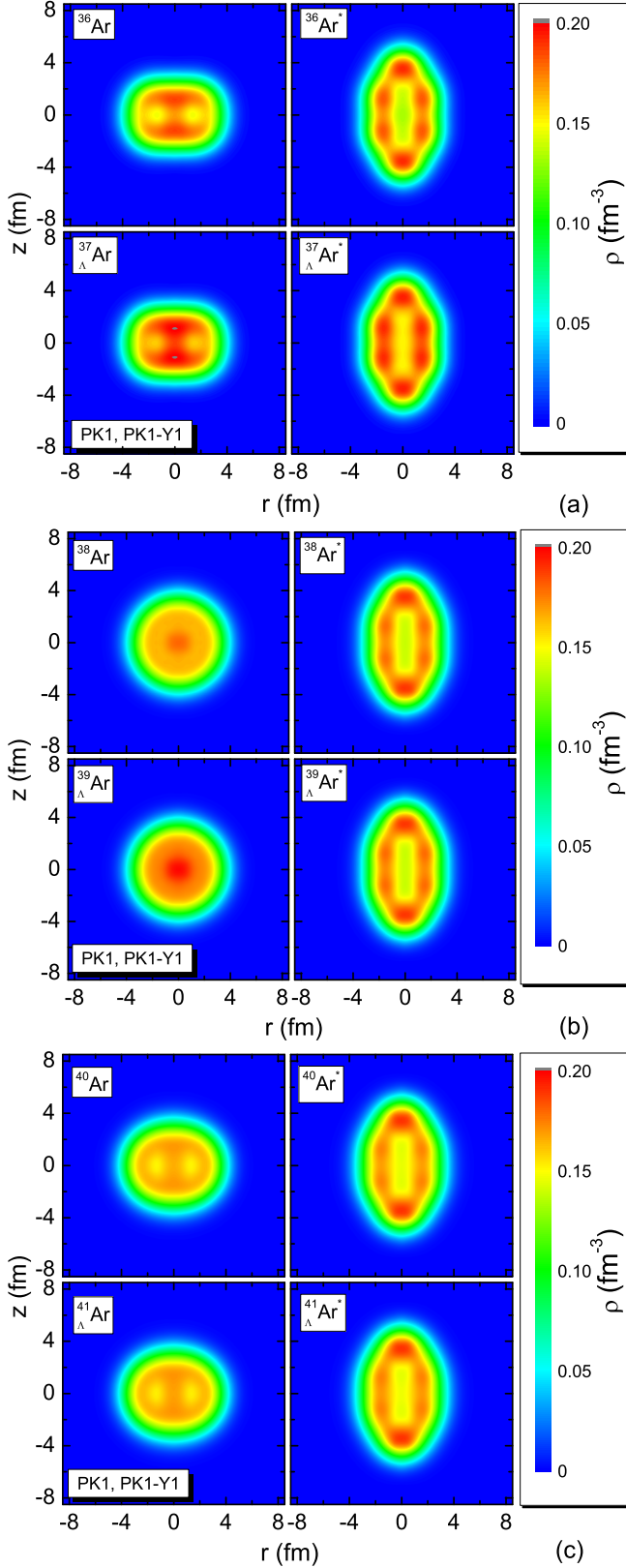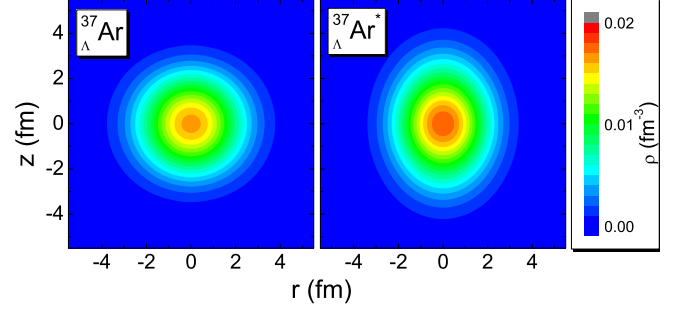
FIG. 3: Two-dimensional density distributions in the r-z plane ($r = \sqrt{x^2 + y^2}$ and z-axis is the symmetric one) for the Λ hyperon in the ground state $^{37}_{\Lambda}$Ar and the SD state $^{37}_{\Lambda}$Ar*.

TABLE III: The probabilities of Λ particle wave function in different Nilsson orbits for $^{37}_{\Lambda}$Ar in ground state and SD state, respectively.

Nilsson levels	GS	SD
$1/2^+$[000]	0.955	0.950
$1/2^+$[220]	0.006	0.038
$1/2^+$[200]	0.034	0.006
$1/2^+$[440]	0.000	0.002

Therefore in the ground state of $^{37}_{\Lambda}$Ar, the overlap between the core and the hyperon wave function is small because the core has an oblate shape while the hyperon is almost spherical. However, in the SD state of $^{37}_{\Lambda}$Ar, the density distribution of the Λ hyperon is stretched substantially along the z-axis and the quadrupole deformation parameter $\beta_{\Lambda} = 0.172$ (see Table I). The probabilities of the hyperon wave function in different Nilsson orbits are given in Table III for the ground and SD states in $^{37}_{\Lambda}$Ar. It is seen that the hyperon wave function embedded in the SD state has larger high-N components (even $4\hbar\omega$ excitation) than in the ground state. These higher-N components with $m_l = 0$ corresponds to larger prolate shape [52, 53] and results in a larger overlap between the hyperon and the core in $^{37}_{\Lambda}$Ar*. Since the SD density distribution shows a localization feature with a ring shape near the surface and a hole structure with low density at the center and the radial coordinate r is included in the integrand, i.e., $r\rho_{\text{core}}(r,z)\rho_{\Lambda}(r,z)$ in Eq. (11), it is natural that the overlap I_{overlap} is larger in the SD state than that in the ground state of $^{37}_{\Lambda}$Ar.

To clarify the relation between the large Λ-separation energy in the SD state and the localization feature of the core nucleus, we investigate nuclei which have SD minima in their potential energy surfaces such as ^{32}S, ^{40}Ca, ^{56}Ni, and ^{60}Zn and the corresponding Λ hypernuclei. Among these nuclei, as shown in Fig. 4, for ^{40}Ca the SD state has a localization in its density profile with a ring shape and in other SD states there are no localization effects. Then it is expected that the localization in the SD state causes again a large overlap between the core and the hyperon wave function and, as a result, the
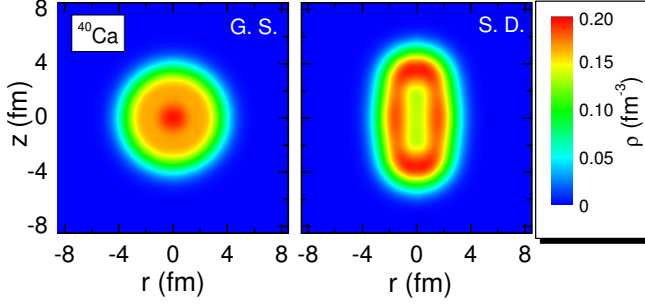

FIG. 2: Two-dimensional density distributions in the r-z plane ($r = \sqrt{x^2 + y^2}$ and z-axis is the symmetric one) for (a) ^{36}Ar and $^{37}_{\Lambda}$Ar and (b) ^{38}Ar and $^{39}_{\Lambda}$Ar and (c) ^{40}Ar and $^{41}_{\Lambda}$Ar The asterisks are marked for SD states.

FIG. 4: Two-dimensional density distributions in the r-z plane ($r = \sqrt{x^2 + y^2}$ and z-axis is the symmetric one) in the ground state and the SD state of ^{40}Ca.

Λ separation energy of the SD state becomes larger than that of the ground state. On the other hand, it is likely that since other isotopes, ^{32}S, ^{56}Ni, and ^{60}Zn have non-localized core densities, the Λ separation energies in SD states should be smaller than those in the ground states. In Table II, we give the overlaps I_{overlap} together the deformation parameter β_2, the binding energy E, and Λ separation energy S_Λ of these Λ hypernuclei. For $^{41}_{\Lambda}$Ca, the overlap I_{overlap} in the SD state is indeed larger than that in the ground state, so is S_Λ. However, for $^{33}_{\Lambda}$S, $^{57}_{\Lambda}$Ni, and $^{61}_{\Lambda}$Zn, the overlap between the hyperon and the SD core is smaller than that of the ground state which is either normally deformed or spherical. Then the Λ separation energy is larger for the smaller deformed state than for the SD state.

From the above discussions, we conclude that the localization in the SD density tends to derive an appreciable deformation in the hyperon wave function (see Fig. 3) and a larger overlap between the core and the hyperon which in turn results in a larger Λ separation energy. However, if in the SD state there is no localization in the core density, the overlap between the core and the hyperon is smaller in the SD state than that in the ground state, which results in a larger Λ separation energy in the latter. These conclusions have been partly demonstrated in recent AMD model calculations by Isaka et al.: The density for the SD state in ^{36}Ar does not show

the localization feature and the Λ separation energy of the ground state is larger than that of the SD state in $^{37}_{\Lambda}$Ar [54] which is contradictory to the present results from RMF models. It would be very interesting to study the localization feature of different mean field models for nuclear SD states.

IV. SUMMARY

We studied the SD states and corresponding SD hypernuclei of Ar isotopes by using the RMF model. We found that the density profiles of SD states in Ar isotopes show a strong localization with a ring structure near the surface, while the central part of the density is dilute showing a hole structure. The strong localization of the SD state is also found in ^{40}Ca. This localization feature of the SD density induces an appreciable deformation in the hyperon wave function of the SD hypernuclei. Then the Λ separation energy of SD state becomes larger than that of normally deformed or spherical ground state. This feature is different from that found in other nuclei such as $^{33}_{\Lambda}$S, $^{57}_{\Lambda}$Ni and $^{61}_{\Lambda}$Zn in which the Λ separation energy of the SD state is smaller. In this context, the measurement of the Λ separation energy would provide an important information on the localization of the density profile of SD states.

[1] T. Motoba, H. Bando, and K. Ikeda, Prog. Theor. Phys. **70**, 189 (1983).

[2] T. Motoba, H. Bando, K. Ikeda, and T. Yamada, Prog. Theo. Phys. Supp. **81**, 42 (1985).

[3] E. Hiyama, M. Kamimura, T. Motoba, T. Yamada, and Y. Yamamoto, Phys. Rev. C **53**, 2075 (1996).

[4] E. Hiyama, M. Kamimura, K. Miyazaki, and T. Motoba, Phys. Rev. C **59**, 2351 (1999).

[5] E. Hiyama, M. Kamimura, T. Motoba, T. Yamada, and Y. Yamamoto, Prog. Theo. Phys. **97**, 881 (1997).

[6] E. Hiyama and Y. Yamamoto, Prog. Theo. Phys. **128**, 105 (2012).

[7] Y. Zhang, E. Hiyama, and Y. Yamamoto, Nucl. Phys. A **881**, 288 (2012).

[8] M. Isaka, M. Kimura, A. Dote, and A. Ohnishi, Phys. Rev. C **83**, 044323 (2011).

[9] X.-R. Zhou, H.-J. Schulze, H. Sagawa, C.-X. Wu, and E.-G. Zhao, Phys. Rev. C **76**, 034312 (2007).

[10] M. T. Win and K. Hagino, Phys. Rev. C **78**, 054311 (2008).

[11] H.-J. Schulze, M. T. Win, K. Hagino, and H. S. Sagawa, Prog. Theo. Phys. **123**, 569 (2010).

[12] M. T. Win, K. Hagino, and T. Koike, Phys. Rev. C **83**, 014301 (2011).

[13] B.-N. Lu, E.-G. Zhao, and S.-G. Zhou, Phys. Rev. C **84**, 014328 (2011).

[14] C. E. Svensson, A. O. Macchiavelli, A. Juodagalvis, A. Poves, I. Ragnarsson, S. Aberg, D. E. Appelbe, R. A. E. Austin, G. C. Ball, M. P. Carpenter, E. Caurier, R. M. Clark, M. Cromaz, M. A. Deleplanque, R. M. Diamond, P. Fallon, R. V. F. Janssens, G. J. Lane, I. Y. Lee, F. Nowacki, D. G. Sarantites, F. S. Stephens, K. Vetter, and D. Ward, Phys. Rev. C **63**, 061301(R) (2001).

[15] E. Ideguchi, D. G. Sarantites, W. Reviol, A. V. Afanasjev, M. Devlin, C. Baktash, R. V. F. Janssens, D. Rudolph, A. Axelsson, M. P. Carpenter, A. Galindo-Uribarri, D. R. LaFosse, T. Lauritsen, F. Lerma, C. J. Lister, P. Reiter, D. Seweryniak, M. Weiszflog, and J. N. Wilson, Phys. Rev. Lett. **87**, 222501 (2001).

[16] C. D. O'Leary, M. A. Bentley, B. A. Brown, D. E. Appelbe, R. A. Bark, D. M. Cullen, S. Erturk, A. Maj, and A. C. Merchant, Phys. Rev. C **61**, 064314 (2000).

[17] T. Inakura, S. Mizutori, M. Yamagami, and K. Matsuyanagi, Nucl. Phys. A **710**, 261 (2002).

[18] M. Bender, H. Flocard, and P. H. Heenen, Phys. Rev. C **68**, 044321 (2003).

[19] R. R. Rodriguez-guzman, J. L. Egido, and L. M. Robledo, Int. J. Mod. Phys. E **13**, 139 (2004).

[20] T. Nikšić, D. Vretenar, and P. Ring, Phys. Rev. C **73**, 034308 (2006).

[21] T. Niksic, D. Vretenar, and P. Ring, Phys. Rev. C **74**, 064309 (2006).

[22] T. Nikšić, Z. P. Li, D. Vretenar, L. Prochniak, J. Meng, and P. Ring, Phys. Rev. C **79**, 034303 (2009).

[23] M. Isaka, K. Fukukawa, M. Kimura, E. Hiyama, H. Sagawa, and Y. Yamamoto, Phys. Rev. C **89**, 024310 (2014).

[24] J.-P. Ebran, E. Khan, T. Nikšić, and D. Vretenar, Nature **487**, 341 (2012).

[25] J.-P. Ebran, E. Khan, T. Niksic, and D. Vretenar, Phys. Rev. C **87**, 044307 (2013).

[26] B.-N. Lu, J. Zhao, E.-G. Zhao, and S.-G. Zhou, Phys. Rev. C **89**, 014323 (2014).

[27] B.-N. Lu, E.-G. Zhao, and S.-G. Zhou, Phys. Rev. C **85**, 011301(R) (2012).

[28] J. Zhao, B.-N. Lu, E.-G. Zhao, and S.-G. Zhou, Phys. Rev. C **86**, 057304 (2012).

[29] J. Zhao et al., "Triple-humped barriers in actinides from multidimensionally-constrained relativistic mean field models," to be published.

[30] Y. K. Gambhir, P. Ring, and A. Thimet, Ann. Phys. (NY) **198**, 132 (1990).

[31] B. D. Serot and J. D. Walecka, Adv. Nucl. Phys. **16**, 1 (1986).

[32] P. G. Reinhard, Rep. Prog. Phys. **52**, 439 (1989).

[33] P. Ring, Prog. Part. Nucl. Phys. **37**, 193 (1996).

[34] M. Bender, P.-H. Heenen, and P.-G. Reinhard, Rev. Mod. Phys. **75**, 121 (2003).

[35] D. Vretenar, A. V. Afanasjev, G. A. Lalazissis, and P. Ring, Phys. Rep. **409**, 101 (2005).

[36] J. Meng, H. Toki, S. G. Zhou, S. Q. Zhang, W. H. Long, and L. S. Geng, Prog. Part. Nucl. Phys. **57**, 470 (2006).

[37] T. Nikšić, D. Vretenar, and P. Ring, Prog. Part. Nucl. Phys. **66**, 519 (2011).

[38] B. K. Jennings, Phys. Lett. B **246**, 325 (1990).

[39] Y. Akaishi, T. Harada, S. Shinmura, and K. S. Myint, Phys. Rev. Lett. **84**, 3539 (2000).

[40] D. Millener, Nucl. Phys. A **804**, 84 (2008).

[41] W. Long, J. Meng, N. V. Giai, and S.-G. Zhou, Phys. Rev. C **69**, 034319 (2004).

[42] C. Y. Song, J. M. Yao, H. F. Lü, and J. Meng, Int. J. Mod. Phys. E **19**, 2538 (2010).

[43] X.-S. Wang, H.-Y. Sang, J.-H. Wang, and H.-F. Lü, Commun. Theor. Phys. **60**, 479 (2013).

[44] P. Ring and P. Schuck, *The Nuclear Many-Body Problem* (Springer-Verlag, Berlin/Heidelberg/New York, 1980).

[45] M. Bender, K. Rutz, P.-G. Reinhard, and J. A. Maruhn, Eur. Phys. J. A **7**, 467 (2000).

[46] Y. Tian, Z. Ma, and P. Ring, Phys. Lett. B **676**, 44 (2009).

[47] Y. Tian, Z.-y. Ma, and P. Ring, Phys. Rev. C **80**, 024313 (2009).

[48] T. Nikšić, P. Ring, D. Vretenar, Y. Tian, and Z.-y. Ma, Phys. Rev. C **81**, 054318 (2010).

[49] G. Audi, F. G. Kondev, M. Wang, B. Pfeiffer, X. Sun, J. Blachot, and M. MacCormick, Chin. Phys. C **36**, 1157 (2012).

[50] G. Audi, M. Wang, A. H. Wapstra, F. G. Kondev, M. MacCormick, X. X., and B. Pfeiffer, Chin. Phys. C **36**, 1287 (2012).

[51] M. Wang, G. Audi, A. H. Wapstra, F. G. Kondev, M. MacCormick, X. X., and B. Pfeiffer, Chin. Phys. C **36**, 1603 (2012).

[52] S.-G. Zhou, J. Meng, P. Ring, and E.-G. Zhao, Phys. Rev. C **82**, 011301(R) (2010).

[53] L. Li, J. Meng, P. Ring, E.-G. Zhao, and S.-G. Zhou, Phys. Rev. C **85**, 024312 (2012).

[54] M. Isaka, to be published.